Title

Ultrafast Relaxations in Ruthenium Polypyridyl Chromophores Determined by Stochastic Kinetics Simulations

Journal

The Journal of Physical Chemistry B, 124(28)

ISSN

1520-6106

Authors

Cheshire, Thomas P

Brennaman, M Kyle

Giokas, Paul G

et al.

Publication Date

2020-07-16

DOI

10.1021/acs.jpcb.0c03110

Peer reviewed

Ultrafast Relaxations in Ruthenium Polypyridyl Chromophores Determined by Stochastic Kinetics Simulations

Thomas P. Cheshire[a], M. Kyle Brennaman[b], Paul G. Giokas[c], David F. Zigler[d], Andrew M. Moran[b], John M. Papanikolas[b], Gerald J. Meyer[b], Thomas J. Meyer[b], and Frances A. Houle[a*]

[a] Chemical Sciences Division, Lawrence Berkeley National Laboratory Berkeley, CA 94720

[b] Department of Chemistry, University of North Carolina at Chapel Hill, Chapel Hill, NC 27599

[c] Coherent Inc., Santa Clara, CA 95054

[d] Chemistry & Biochemistry Department, California Polytechnic State University, San Luis Obispo, CA 93407

KEYWORDS: Kinetics, metal to ligand charge transfer, chromophore, transient absorption, stochastic simulations

ABSTRACT: Maximizing the efficiency of solar energy conversion using dye assemblies rests on understanding where the energy goes following absorption. Transient spectroscopies in solution are useful for this purpose, and the time-resolved data are usually analyzed with a sum of exponentials. This treatment assumes that dynamic events are well separated in time, and that the resulting exponential pre-factors and phenomenological lifetimes are related directly to primary physical values. Such assumptions break down for coincident absorption, emission, and excited state relaxation that occur in transient absorption and photoluminescence of tris(2,2'-bipyridine)ruthenium(2+) derivatives, confounding the physical meaning of the reported lifetimes. In this work, we use inductive modeling and stochastic chemical kinetics to develop a detailed description of the primary ultrafast photophysics in transient spectroscopies of a series of Ru dyes, as an alternative to sums of exponentials analysis. Commonly invoked 3-level schemes involving absorption, intersystem crossing, and slow non-radiative relaxation and incoherent emission to the ground state cannot reproduce the experimentally measured spectra. The kinetics simulations reveal that ultrafast decay from the singlet excited state manifold to the ground state competes with intersystem crossing to the triplet excited state, whose efficiency as determined to be less than unity. The populations predicted by the simulations are used to estimate the magnitudes of transition dipoles for excited state excitations, and evaluate the influence of specific ligands. The mechanistic framework and methodology presented here are entirely general, applicable to other dye classes, and can be extended to include charge injection by molecules bound to semiconductor surfaces.

1. Introduction

Photoexcitation of molecular chromophores supported on conducting substrates provides a means of converting sunlight into electrons, which can then generate electricity or be converted further into chemical energy. The dynamics of chromophore excitation and charge injection are much studied, with a goal of improving solar energy conversion efficiency. This has led to a significant body of work on chromophores used in dye sensitized solar cells (DSSC), with early work centered on organic dyes.[1-5] The photophysical properties of these dyes govern electron injection into the substrate, making the choice of the chromophore a definitive factor in cell design. The nature of energy relaxations and the exact timing of charge injection into the semiconductor relative to other processes occurring in the cells are not fully quantified, although recent studies have made significant progress toward this goal.[6-10] It is important to understand these fundamental processes

in greater detail. In this work, we focus specifically on quantifying the kinetics of excitations that precede charge injection, revealed by simulations of time-resolved spectroscopies in solution. This provides an understanding of processes that occur when no charge injection is possible, thereby establishing a mechanistic platform that can be extended to include adsorbed dye photophysical processes.

While many dyes have been investigated,[11-14] a few have emerged that are useful models amenable to deeper study because of the wealth of data available for them. Here, we focus on tris(2,2'-bipyridine)ruthenium(2+) (RuBPY) and its derivatives. RuBPY is of particular interest as an energy conversion chromophore due to a large metal-to-ligand charge transfer (MLCT) absorption band in the 400 - 500 nm range, stability in adjacent redox states, and excited state lifetimes on the microsecond timescale. The literature provides important information on the details of the energy transformations involved, and how a 3-state description for excitation and relaxation has been developed, illustrated in Figure 1. Following light absorption from the singlet ground state, the ^{1}MLCT undergoes intersystem crossing (ISC) to a ^{3}MLCT. The involvement of two MLCT states contributes to the long-lived excited state population. The earliest studies of RuBPY aimed to assign the electronic states participating in absorption and emission spectra, with the help of theoretical predictions.[15-19] By the 1970s, a consensus had been established that the absorption band in the blue region of the spectra originated from singlet to singlet MLCT transitions and the intense luminescence in the red region of the spectra involved a spin forbidden transition. Though the exact nature of the emitting triplet state was still under debate, the discussion turned to the transitions between excited states, such as internal conversion (IC) and ISC.[20] Early on, the assertion by Lytle and Hercules that ISC efficiency (ϕ_{ISC}) is near unity for RuBPY found general acceptance,[21-24] although some evidence suggested that there is only a lower bound to ϕ_{ISC} of ~ 0.5.[25] Yet additional studies using new methods for determining ϕ_{ISC} seemed to confirm that RuBPY photoexcited into the ^{1}MLCT manifold only depopulates through ISC.[26-28]

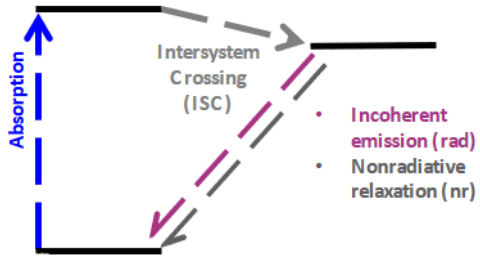

Figure 1. A Jablonski diagram illustrates a simple 3-state system. Absorption (blue) from the ground state to an excited state singlet is followed by ISC (light gray) to a triplet state. Incoherent emission (rose) and non-radiative relaxation (dark gray) return population from the triplet state to the ground state.

Advancements in laser technology made shorter pulses possible, enabling transient spectroscopies that deliver improved time resolution in experiments and precision of estimated rate coefficients for non-radiative pathways. To extract kinetic information from transient optical measurements such as absorption or photoluminescence, a basic mechanism is assumed. The simplest one for ruthenium polypyridyl chromophores entails the 3-level system in Figure 1. Relaxations within the singlet manifold prior to ISC are fast. Whereas initially only an upper bound on the lifetime of ISC of <10 ps was estimated, researchers have since used lifetimes to place it within 15 fs to 100 fs.[29-30] Damrauer et al. proposed that intramolecular vibrational redistribution (IVR) and IC within the singlet manifold are faster processes than ISC to the triplet state, but added such channels likely cannot be decoupled. The excited state population within the triplet manifold is long-lived and relaxes to the ground state via incoherent emission and non-radiative relaxation on the microsecond timescale.

Interpretation of spectroscopic data in terms of this 3-state scheme therefore assumes that 1) absorption and vibrational relaxation are fast compared to ISC, 2) ISC efficiency is unity, and 3) radiative and non-radiative relaxation are rate limiting steps for ground state repopulation. Additionally, 1) means that the excited singlet state involved in ISC is assumed to be fully populated by the pump pulse before transition to the triplet manifold commences. However, in most time-resolved spectroscopic experiments, the duration of the pump pulse is finite and is coincident with ultrafast dark transitions. That is, the excited singlet state is being populated and depopulated simultaneously, and optical signals combine multiple simultaneous processes. The kinetics of this 3-state scheme are usually quantified by neglecting these physics, and assuming all state-to-state transitions are first-order processes. A number of additional approximations are involved in this treatment: in particular, common methods for analyzing transient absorption (TA) signals do not incorporate the initial absorption of the pump pulse, and assume the form of a multi-exponential decay for the ground state bleach (GSB) and the excited state absorptions (ESA), Equation (1),

$$S_{\omega}(\tau) = \sum_{i} A_i \cdot \exp\left[-k_i \cdot \tau\right] \quad (1)$$

where $S_w(\tau)$ is the time dependent signal at frequency ω (cm^{-1}), A_i is the amplitude of the i^{th} fitting component, τ is time (s) and k_i (s^{-1}), are phenomenological rate coefficients. The amplitudes encode initial concentrations and ratios of the phenomenological lifetimes, and are proportional to the signal, a unitless quantity. The phenomenological rate coefficients can combine several primary rate coefficients, which cannot be separated without additional information. This brings into question whether a measured decay curve can be interpreted as being dominated by a primary kinetic step even in a simple 3-state scheme.

An additional complication is that the specific nature of the electronic states involved in measurements of the RuBPY excitation-relaxation mechanisms are not fully determined. Early investigators referred to states as being "singlet" or "triplet". [31-32] Theory and computation suggests significant mixing of spin states, making purported multiplicity more of a convention than a physically meaningful property.[33-34] The localization or delocalization of the excitations on ligands has also been scrutinized, and has implications for whether electronic relaxation between excited states is described as interligand electron transfer (IL ET) or IC.[30, 35-41]

Given the complexity of the processes probed by RuBPY measurements, it is evident that simple analyses will be challenging to use to understand primary photophysical processes. Incorporating the optical transitions into a kinetic framework sidesteps the drawbacks encountered in a sum of exponentials analysis (Equation 1), and enables direct connection to any non-radiative transitions, which are difficult to access using that treatment. We have taken a new approach to characterizing the full process of light absorption and relaxation, using inductive kinetic modeling techniques[42] to discover a predictive mechanism consistent with experimental data for ultrafast TA and time-resolved photoluminescence (TRPL) measurements for dyes dissolved in a solvent at room temperature. Inductive modeling involves starting from the simplest possible description of a system's processes, for example Figure 1, and using it to predict time-dependent signals for comparison to experimental data. New photophysics are only added when the model cannot reproduce observations. The result is a model that contains only elements that have been demonstrated to be kinetically significant. Accordingly, the mechanistic scheme described here contains all the elementary excitation and relaxation steps for the photophysics occurring under broadband illumination. It is extendable to other systems and dye environments, and represents a new paradigm for treatment of spectroscopic data.

2. Methods

2.1. Experimental Data Used in this Work

For this work, we compiled and reanalyzed data reported in previous studies[43-44] as well as unpublished data from the same investigations. This allowed us to assemble sufficient independent types of information to test whether the kinetic scheme is self-consistent and capable of reproducing multiple experimental observations. Important details of the measurements used in the simulations are listed here.

Photoluminescence: For TRPL, 0.150 mM solutions of the ruthenium complexes in 0.1 M $HClO_4$ were excited by an 80-ps pulse centered around 444 nm and monitored by time-correlated single-photon counting.[44] Extinction coefficients were also taken from this study.

Transient absorption: The TA data for 4 mM solutions of six ruthenium dyes in methanol analyzed in this study were collected by Giokas et al.[43] A 45-fs pump pulse centered at 400 nm with ~1000 cm^{-1} linewidth interacts with approximately 10% of the molecules in a microjet of solution. Following the experimentally controlled delay, the broadband probe perturbs the system to induce linear and third-order responses. A fuller description can be found in ref.[43] TA data were prepared for analysis by commonly used methods.[45] 15 to 30 scans per chromophore were averaged. Arrival of the broadband probe pulse at all wavelengths was corrected for numerically (i.e. chirp correction). The baseline of the TA signal was removed by subtracting out the mean difference in absorption $\boldsymbol{A}$ of pump on and pump off scans at several negative delay points. Time-zero was defined at the point the GSB attained 2/3 peak intensity, ~550 fs greater than time-zero determined by chirp correction.

2.2. Simulation Software

The kinetics simulations were performed using the open access software Kinetiscope.[46] Unlike familiar kinetic Monte Carlo methods, Kinetiscope uses a core algorithm that tracks an ensemble of particles in event space rather than individual particles of an ensemble in physical space, and generates an absolute time base for comparison to experimental data. It is a rigorous solution to the master equation, and offers advantages over differential equation solvers when large dynamic ranges of timescales and concentrations are involved and portions of the reaction mechanism are not well known. The algorithm was first reported by Bunker,[47] and later by Gillespie, who developed the full mathematical foundation.[48] The code package

has the ability to specify time-dependent variables that have been used in this work to simulate the probe pulse shape and time delays. Because the simulation method is particle-based, rather than coupled differential equation based, it allows insertion of marker species throughout the mechanistic steps without affecting the accuracy of the simulation. These marker species are invaluable for analysis of which kinetic pathways are contributing to which parts of the signal, as will be evident below where, for example, the simulated and observed GSB signals are compared directly.

3. Model Development

In this section we describe how the kinetic model for dye photophysics is constructed. The resulting kinetic framework specifically and quantitatively reproduces ultrafast TA spectroscopy data on RuBPY chromophores for direct comparison to experiment. Wherever possible, the mechanism is constructed using experimental data. They include rate constants derived from linear spectroscopy, photoluminescence decays at long times, absolute dye concentrations in solution, and specific details of the pump and probe pulses that drive and probe the dynamical processes. Rate coefficients not available from direct measurements are estimated using simulations, with the criterion that the calculations reproduce a set of measurements quantitatively in ΔA and time over the full time span of the measurements (fs to μs). This is done by converting calculated concentration *vs* time data into optical signals. Throughout the description of our model, we often invoke the labels "singlet" and "triplet". As noted in the introduction, there is likely significant mixing between these states, and this terminology is meant as shorthand for "primarily singlet in character" and "primarily triplet in character" respectively. As noted above, the RuBPY dyes are a useful model system: in addition to permitting construction of a general kinetic framework for dye photophysics and assessing its generality, the availability of data for a series of 6 structurally related chromophores enables us to evaluate the influence of ligand structure on the photophysics, including estimation of transition dipole magnitudes, in a systematic way. While this study focuses only on one dye family, the methodology is entirely general and can be used for any chromophore where comparable data are available.

3.1. Chromophores

Figure 2 shows the RuBPY derivatives used for the computational treatment developed here, with RuP chosen as the base system for model construction. These structurally related, molecular light-absorbers share common electronic structures and have readily available spectroscopic data. RuBPY and its derivatives exhibit similar optical transitions, and

the ruthenium center imposes a large SOC increasing the probability of ISC.[34, 49] For this set of complexes, the normal modes of each bipyridine ligand are comparable, and the addition of phosphonates and methylphosphonates only slightly perturbs both nuclear coordinates and frequencies.[43] It is reasonable to assume that this class of dyes shares promoting modes for transitions. Simulations of transient spectroscopy measurements for all dyes using the mechanism for RuP results in good agreement with experiment, as will be presented below.

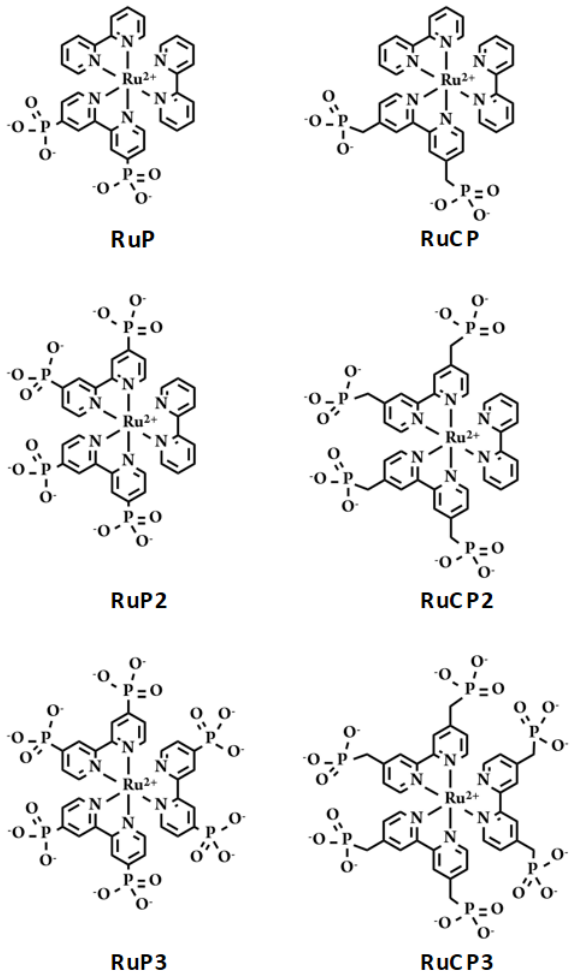

Figure 2. Ruthenium polypyridyl dyes: the number represents the number of phosphonated ligands and the 'C' indicates methyl spacers between the ligand and phosphonates.

3.2. Modeling Transient Absorption

Because of its well-defined signal components, TA is an indispensable technique for understanding dark transitions accompanying absorption and emission of light. Excited state emission (ESE) and GSB can inform how initially prepared states relax and how the ground state is repopulated, while ESAs primarily provide insights into downstream processes. TA

is performed as a difference in absorption experiment, subtracting the signal of a probe scan acquired without a 'pump' laser pulse from the measured signal of a probe scan with 'pump' laser excitation. The result is the pump-probe signal. The sum of the wavevectors and frequencies of the laser pulses interacting with dye define the signal components, and therefore the type of nonlinear signal measured.

To create a kinetic model in which TA signals can be simulated, it is instructive to first consider how the pump-probe experiment is performed and the nature of the interactions between solute and the impinging laser pulses. Figure 3 depicts the photophysical pathways of ruthenium polypyridyl complexes. The monochromatic pump pulse excites a fraction of the population from the ground state into one or more excited states and perturbs a fraction of the ground state into non-equilibrium conditions such as multiple quanta vibrational states. The broadband probe pulse does not spectrally overlap the pump pulse in the data presented in this study; however, signal can be induced from the ground state, excited singlet states, and excited triplet state, i.e. all populations possessing non-negligible probability of an optical transition within the broadband spectral range. The temporal delay between the pump and probe pulses allows information to be obtained on dynamics coupling these states within the system, which can progress to varying extents depending on the duration of the delay. Coincident pump and probe pulses can induce undesirable nonlinearities, other than the pump-probe signal, that make analysis at time zero extremely challenging. These so-called coherent artifacts, for example two-photon absorption and Raman scattering, are assumed to be negligible in this study. The pump and probe pulses are well-separated at the defined time zero (when the GSB attains 2/3 intensity), and the carrier frequency of the pump laser pulse is >2500 cm^{-1} than the highest probe pulse frequency that has significant intensity. Therefore, coherent artifacts are not depicted in Figure 3.

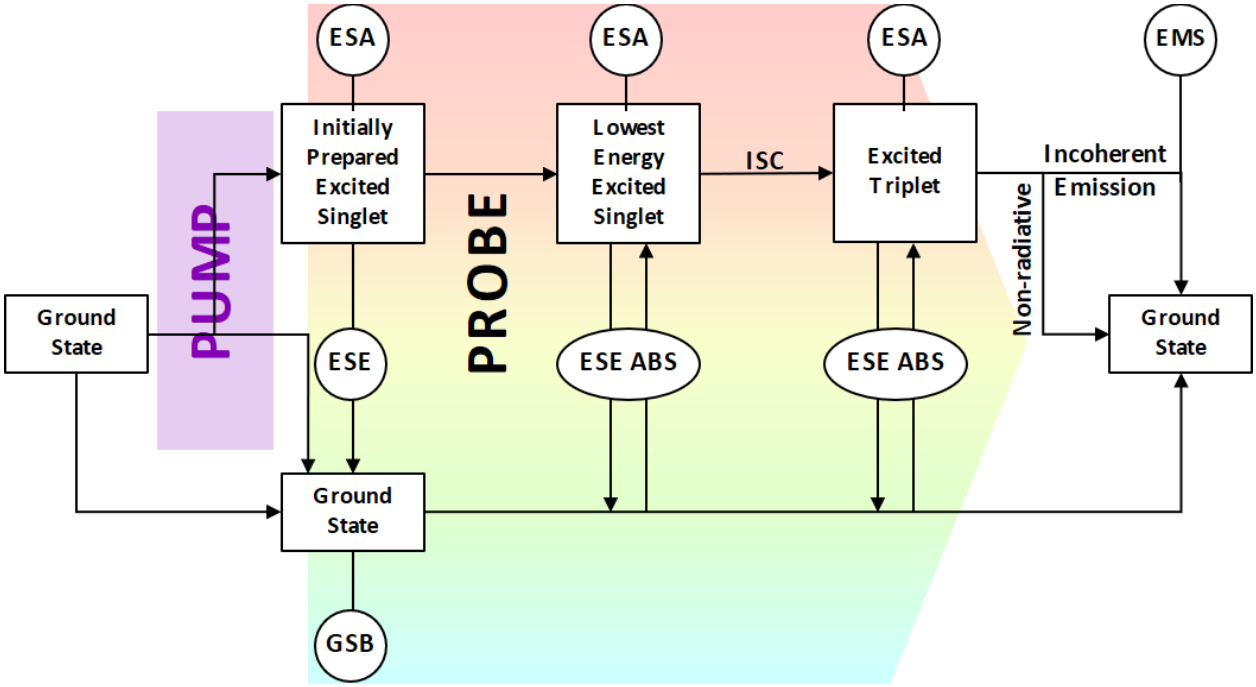

Figure 3. Observable signals of a 4-level system that can undergo relaxation between excited states and between an excited state and the ground state by TA spectroscopy. The pump pulse excites a fraction of the ground state population to the initially prepared excited singlet state. Interactions with the probe that are not accompanied by electronic transitions include the ground state bleach (GSB) and excited state absorptions (ESA) signal components. The probe pulse can induce absorption (ABS) from the ground state and stimulated emission (ESE) from excited states. Relaxation between singlet states could be intramolecular vibrational relaxation (IVR), interligand electron transfer (ILET), or internal conversion (IC). Following the initial excitation, excited state populations can undergo intersystem crossing (ISC) from singlet to triplet states. The ground state is repopulated, at long times, through non-radiative relaxation and incoherent emission (EMS).

The population in the ground state, interacting with the probe, governs the GSB signal component. Absorption from the ground state to an excited state and stimulated emission from the excited state down to the ground state overlap the GSB and contribute additively to it. There is nonzero probability, as observed in the linear absorption spectrum in Figure 4, of absorption and stimulated emission between the ground state and both excited singlet and triplet states. ESA can also be induced from excited singlet and triplet states. ESA signal components result when electronic coherences between these populations and those of higher energy excited states of unknown multiplicity are instantiated by the probe, followed by relaxation to the lower energy electronically excited state. At very long times, the excited state population that is not stimulated back to the ground state will undergo non-radiative relaxation or incoherent emission. Spontaneously emitted photons radiate in all directions, including along the path of the radiated signal, but the probability of incoherent emission is low compared to ESA signals at nearby wavelengths, and their contribution to the pump-probe signal is negligible.

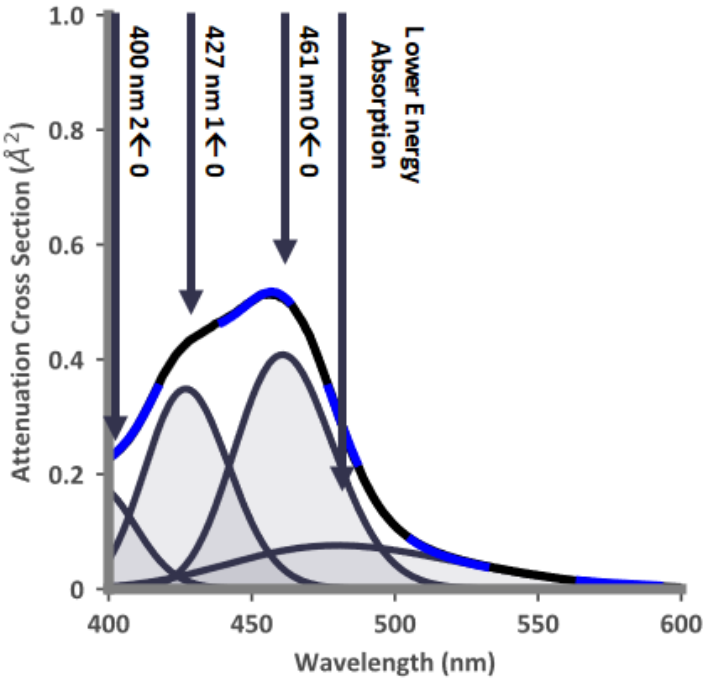

Figure 4. Linear absorption spectrum of chromophore RuP. Vibronic contributions and lower energy absorption are represented as Gaussians, and are shaded in gray. The fit (dashed blue line) and experimental spectrum (solid black) exhibit excellent agreement.

The experimental signal is the delta absorption ΔA which is the negative log of the ratio of intensities of signal measured from the sample with and without the pump pulse. As shown in Equation (2), the pulse intensity I (J s^{-1} m^{-2}) is proportional to the number of photons n at a particular frequency ω. Equation (3) defines ΔA from incident photons at the i^{th} wavelength, where n_i is the maximum possible number of absorbed probe photons and $n_{Signal,on}$ and $n_{Signal,off}$ are probe interactions with and without the pump pulse, respectively.

$$I \propto n\hbar\omega \tag{2}$$

$$\Delta A_i(\tau) = -\log_{10}\left|\frac{n_i - n_{Signal,on}}{n_i - n_{Signal,off}}\right| \tag{3}$$

3.3. Elements of the mechanistic framework

3.3.1. Pump and probe pulses

Simulating TA signals requires 2 pulses separated in time. The pump pulse is modeled as a 45 fs square wave. The TA probe pulse is modeled using an intensity profile $I_{\text{Probe}}(\tau)$. The simulated probe profile is shown in Figure S1. The probe intensity is set at a value that excites ~1% of the ground state population, and the temporal lineshape is approximated from optical Kerr effect measurements.[50] Since absorption of probe photons does not deplete the pulse significantly, the second order rate constant for dye absorption of the probe can be treated as a product of the probe profile and a pseudo first order rate constant calculated from the primary absorption rate constant multiplied by the light intensity. Simulations of a complete pump-probe experiment require a unique simulation for each experimentally controlled delay. A "pump off" simulation is also performed. Cumulative probe interactions are compiled from the set of "pump on" and "pump off" simulations to compute the pump-probe signal.

3.3.2. Primary Optical Transitions and Their Rate Coefficients

Simulating the TA signal as a kinetic mechanism incorporates the following assumptions: 1) electronic decoherence is fast relative to pulse duration, and only total populations in the various states need to be tracked; 2) the broadband probe has comparable intensities at every wavelength (frequency); and 3) states higher in energy than the initially prepared excited state are not significantly populated by either pump or probe interactions. The third assumption is well justified in that to populate higher energy levels would require multiphoton processes within a relatively weak pulse, which has negligible probability. Within these assumptions, we can use spectroscopic data to estimate rate constants for interactions with the probe laser.

The fit to the linear absorption spectrum for chromophore RuP, Figure 4, shows three intense ground state to excited state vibronic transitions and one weaker and broader contribution. The areas of the spectrum components, their full width at half-maxima (FWHM) and their peak intensities, are proportional to rate coefficients for primary steps describing the initial excitations (see Supporting Information, section S2, Equation S1), where the ground state, the lowest energy excited singlet state ($\mathbf{0} \leftarrow \mathbf{0}$), and the excited triplet state (lower energy absorption in the Figure) are defined as $|S0\rangle$, $|X\rangle$, and $|T\rangle$, respectively. In the simplest possible assumption, we equate photoexcitation depicted by the $|X\rangle \leftarrow |S0\rangle$ transition in our framework to the $\mathbf{0} \leftarrow \mathbf{0}$ vibronic transition that dominates the signal at the peak of the linear absorption spectrum in Figure 4.[36, 51] As seen in Figure 3, the 400nm pump pulse accesses higher vibrational excitations within this manifold, but we do not

differentiate these levels at this stage. Equations (4) and (5) are excitations that yield the observed GSB and absorption (ABS) events. *GSB* and *ABS* are marker species that do not participate in the kinetics, but allow the occurrence of these events to be tracked. The rate coefficients for these steps are taken from the $\mathbf{0} \leftarrow \mathbf{0}$ transition, $k_{GSB} = k_{ABS} = 4.8 \cdot 10^{13}\ s^{-1}$.[52] The rate coefficient for direct absorption from the ground state to the excited triplet manifold, Equation (6), was kept constant for all dyes and contributes to less than one third of the interactions between the probe and the ground state population, $1.8 \cdot 10^{13}\ s^{-1}$. *ABS,T* is the marker species that tracks these excitations. For all three excitation steps, the rate coefficient is scaled by $\boldsymbol{I_{Probe}(\tau)}$, the time profile of the probe pulse.

$$|\boldsymbol{S0}\rangle \xrightarrow{|X\rangle, I_{Probe}(\tau)} |\boldsymbol{S0}\rangle + \boldsymbol{GSB} \tag{4}$$

$$|\boldsymbol{S0}\rangle \xrightarrow{I_{Probe}(\tau)} |\boldsymbol{X}\rangle + \boldsymbol{ABS} \tag{5}$$

$$|\boldsymbol{S0}\rangle \xrightarrow{I_{Probe}(\tau)} |\boldsymbol{T}\rangle + \boldsymbol{ABS,T} \tag{6}$$

Figure 5 shows the TA spectrum of dye RuP at 1 ps (solid black), fitted as sum of Gaussians (dashed blue). The data was fit using $\boldsymbol{\Delta A}$ as a function of probe pulse frequency in wavenumbers, but plotted as a function of probe pulse wavelength for convenience. The Gaussians are used to estimate signal contributions from the GSB (shaded gray) and five ESAs (shaded orange). States with primarily singlet or triplet character can generate ESAs. However, from spectroscopic data alone, it is impossible to know the multiplicity of the higher excited state. For that reason, we allow the ESA signal components to come from all excited state populations. Equations (7) and (8) are the mechanistic steps associated with the ESA signal component centered at 521 nm, denoted with marker *ESA,1*, in which the excited states interact with the probe via an implicit higher energy state that we denote as $|\boldsymbol{Z1}\rangle$. The rate coefficient is estimated to be $4.0 \cdot 10^{13}\ s^{-1}$ from the associated signal component of the TA spectrum, in the same way that $\boldsymbol{k_{GSB}}$ was calculated from the linear absorption spectrum, and scaled using the time profile of the probe pulse. Mechanistic steps and rate coefficients for the remaining four ESAs are summarized in Table 1.

$$|\boldsymbol{X}\rangle \xrightarrow{|Z1\rangle, I_{Probe}(\tau)} |\boldsymbol{X}\rangle + \boldsymbol{ESA,1} \tag{7}$$

$$|\boldsymbol{T}\rangle \xrightarrow{|Z1\rangle, I_{Probe}(\tau)} |\boldsymbol{T}\rangle + \boldsymbol{ESA,1} \tag{8}$$

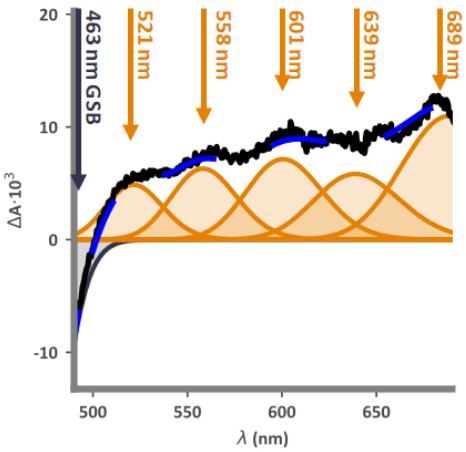

Figure 5. TA spectrum of chromophore RuP at 1 ps from experiment (solid black) and sum of Gaussians (dashed blue). Peaks associated with the GSB and ESAs are shaded in gray and orange respectively.

3.3.3. Photoluminescence: Slow Relaxation Pathways and Rate Coefficients

TRPL simulations involve an initial pump step from the ground state to an electronically excited state, and relaxation events from that state are counted, just as photons are counted experimentally. With the assumption that, at long times, incoherent emission and non-radiative relaxation from the triplet manifold are the only means by which the ground state can be repopulated, photoluminescence (PL) efficiencies ϕ_{PL} and TRPL can be employed to yield excited state lifetimes and estimate relative contributions to excited state decay using the standard analysis, Equation (1). For ruthenium polypyridyl chromophores in solution, the best fit to the absolute emission signal is a single exponential decay, with >95% of the population decaying non-radiatively. The phenomenological rate constant k_{total} is separated into the rate coefficients for radiative (rad) and non-radiative (nr) transitions, as shown in Equations (9)-(13), where the species *rad* is a marker species used to track the number of radiative relaxation events. The values we obtained for RuP, $k_{rad} = 11 \cdot 10^4\ s^{-1}$ and $k_{nr} = 3.2 \cdot 10^6\ s^{-1}$ respectively, agree with previous results.[44] This indicates that thermalization from the excited triplet state into metal centered states is the bottleneck to relaxation; it is assumed relaxation within metal centered states to the ground state is fast[22, 27] and can be neglected in a kinetic scheme. Although the microsecond relaxation pathways, Equations (9) and (10) , have a negligible effect on the femtosecond dynamics, it is imperative to include them in a kinetic framework as an essential handle for evaluating the accuracy of simulated processes that occur earlier in time.

$$|T\rangle \longrightarrow |S0\rangle + rad \tag{9}$$

$$|T\rangle \longrightarrow |S0\rangle \tag{10}$$

$$k_{rad} = \phi_{PL} \cdot k_{total} \tag{11}$$

$$k_{nr} = (1 - \phi_{PL}) \cdot k_{total} \tag{12}$$

$$k_{total} = k_{rad} + k_{nr} \tag{13}$$

3.3.4. Analysis of the GSB Signal

Non-radiative transitions (i.e. IC, IVR, and ISC) are the dominant relaxation pathways following photoexcitation. Dark processes compete kinetically with each other and with absorption and emission events, make direct observation of them impossible. The GSB and ESE signal components are useful spectroscopic handles to obtain information indirectly on non-radiative transitions. Specifically, the peak intensity of the GSB is the turning point at which the rates of depopulation by excitation and repopulation by radiative and non-radiative decay of the ground state are equal.

Starting with processes during the 45 fs pump pulse, approximately 10% of the ground state population is excited, but there is also probability of singlet to triplet conversion during the excitation window. For a 3-level system, ISC necessarily occurs from the lowest energy excited singlet and the excited triplet state, represented in Equation (14). This presumes either the initially prepared excited state and the singlet state that undergoes ISC are identical or that intermediate kinetic events are negligible.

$$|X\rangle \longrightarrow |T\rangle \tag{14}$$

We simulated two simple 3-state models to compare to the experimental decay curve of the GSB in order to understand whether they would be sufficient to describe the kinetics. The first model, model A, includes absorption from the ground state to the lowest energy excited singlet state, ISC, and the slow relaxation pathways from the excited triplet state. The second model, model B, adds to the first model by incorporating the ESE mechanistic steps shown in Equations (15) and (16), where *ESE* and *ESE,T* are marker species that track occurrence of these steps.

$$|X\rangle \xrightarrow{I_{\text{Probe}}(\tau)} |S0\rangle + ESE \tag{15}$$

$$|T\rangle \xrightarrow{I_{Probe}(\tau)} |S0\rangle + ESE, T \quad (16)$$

Rate coefficients for these optical transitions are assumed to be the same as for the absorptions in Equations (5) and (6). As shown in Figure 5, the experimental time traces of the GSB and ESAs decay from peak intensities within 300 fs before leveling off to an asymptotic value on the picosecond timescale. The peak intensity of the GSB predicted by model A, the 3-state model without ESE (solid mustard), and by model B, the 3-state model with ESE (dashed green) behave similarly. The magnitude of the signal increases rapidly prior to time-zero and is comparable to the experimental ΔA (solid black) at 0 fs. Though model B has a very slight decay from the peak intensity, the difference in intensities is negligibly small and would be indistinguishable from noise experimentally. The signal for the 5 ESAs (see panels (B)-(F) in Figure S2) follow the same trends as the GSB.

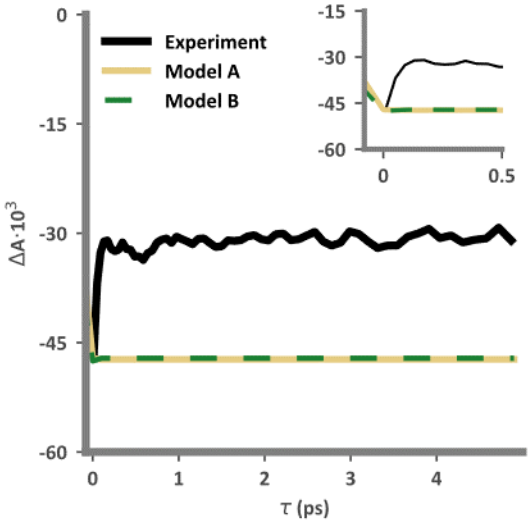

Figure 6. Experimental time trace of the GSB signal component (solid black) compared to simulated decay of model A, the 3-state model without ESE (solid mustard) and model B, the 3-state model with ESE (dashed green). Inset shows -100 fs before and 500 fs after time-zero.

The signal intensities predicted by both models A and B are larger in magnitude than the experimental values for all times >100 fs. This means that the extent of decay of the GSB within the ultrafast regime is not reproduced by either version

of a 3-state model. The ultrafast decay (< 100fs) suggests there is a means by which $|S0\rangle$ is being repopulated that is no longer available beyond the ultrafast regime. To start, we evaluate 2 potential scenarios that could lead to the observed GSB decay. In one scenario, we include a direct relaxation pathway prior to ISC in the reaction scheme. Equation (17) represents an ultrafast non-radiative relaxation (UF-nr) mechanism that would compete with ISC, especially for similar rate coefficients. This process is added to 3-state model A, which becomes model A-UF.

$$|X\rangle \longrightarrow |S0\rangle \tag{17}$$

A second scenario that also could capture the ultrafast decay uses model B, which explicitly includes ESE. The observed GSB decay in Figure 6 of model B is too low at early times. The peak could be more intense if the population involved in singlet to triplet conversion passed through multiple intermediate states, slowing the ISC process. One method for doing this would be to expand model B by separating the excited singlet state into a state $|Y\rangle$, initially prepared by the pump pulse, and the lowest energy excited singlet state that participates in ISC $|X\rangle$. The transition in Equation (18) from state $|Y\rangle$ to state $|X\rangle$ can be understood as a bottleneck to ISC allowing population to accumulate in the initially prepared state, increasing the probability of ESE from state $|Y\rangle$, Equation (19). This converts model B into a 4-state system, model B-4. We did not include the ultrafast decay in Equation (17) in model B-4, but do include the possible generation of ESAs from $|Y\rangle$ in Equation (20).

$$|Y\rangle \longrightarrow |X\rangle \tag{18}$$

$$|Y\rangle \xrightarrow{I_{\mathrm{Probe}}(\tau)} |S0\rangle + ESE \tag{19}$$

$$|Y\rangle \xrightarrow{|Z1\rangle, I_{\mathrm{Probe}}(\tau)} |Y\rangle + ESA,1 \tag{20}$$

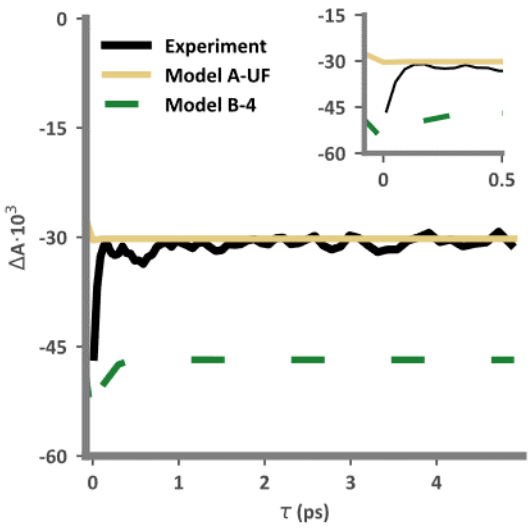

Figure 7. Experimental time trace of the GSB signal component (solid black) is compared to simulated decay of 3-state model with ESE (model A-UF) (solid mustard) and a 4-state model (model B-4) (dashed green). The inset shows -100fs before and 500 fs after time zero.

The results of simulating these proposed models are shown in Figure 6. It is evident that neither the 3-state model A-UF (solid mustard) nor the 4-state model B-4 (dashed green) in Figure 7 are in good agreement with the experimental GSB signal (solid black). Model A-UF does not exhibit decay on the femtosecond timescale, though intensities match observations at times >500 fs. As shown in Figure S3, the ESAs in panels (B)-(F) exhibit better agreement with the experimental decay, however. Model B-4 has the correct ultrafast peak followed by a decay, but it predicts GSB intensities that are much larger than measured values beyond 150 fs.

Models A-UF and B-4, which individually do not agree with experimental observations at all times, do agree with experiment over specific, and entirely separate, time regimes. This suggests that the two can be merged to obtain a better description over the entire time span of the measurements. We denote the combined model as Model C. We constructed the photophysical mechanism by first finding a rate coefficient for the ultrafast decay from $|\boldsymbol{X}\rangle$, Equation (17), which contributes to the repopulation of the ground state and reduces GSB intensity at larger delay times. Holding this part of the reaction scheme as fixed, we then added Equation (18), using the experimentally constrained extent of excitation. Model C

says that the characteristic decay of the GSB is attributable to stimulated emission, relaxation within the singlet manifold, and transitions out of singlet manifold.

Each state invoked in Model C can be either a single state or a set of closely related states. The transition step from the ground state to the lowest energy singlet state can be a Franck-Condon transition, or multiple transitions involving nearly degenerate electronically excited energy levels and a distribution of populated vibrational modes in the ground state. The available experimental TA data do not have the spectral resolution to discern such subtle heterogeneity, therefore we do not include it. The success of Model C depends only on including broadly defined transitions, and is independent of the exact identity of each state. The model can be readily extended to include complex excitations as data become available.

3.4. Summary of the Kinetic Framework

The mechanistic steps and rate coefficients for the full photophysical excitation-decay mechanism for RuP are collected in Table 1. A diagram showing the transitions is shown in Figure 8. This kinetic framework contains all processes that are both necessary and sufficient to describe the photophysics of dye RuP, and to simulate the femtosecond TA and TRP L spectra at our current level of understanding. It is easily extendable to accommodate new knowledge as it becomes available through theory and experiment.

Table 1. Mechanistic steps and estimated rate coefficients from experimental data and simulations of time-resolved spectroscopies for RuP as described by Model C

	Rate Coefficients	Experiment (s^{-1})	Simulation (s^{-1})
$\|S0\rangle \xrightarrow{h\nu_{Pump}} \|Y\rangle$	k_{Pumps}	---	[*] $8.9 \cdot 10^{8}$
$\|S0\rangle \xrightarrow{\|X\rangle, I_{Probe}(\tau)} \|S0\rangle + GSB$	k_{GSB}	[a] $4.8 \cdot 10^{13}$	$4.8 \cdot 10^{13}$
$\|S0\rangle \xrightarrow{I_{Probe}(\tau)} \|X\rangle + ABS$	k_{ABS}		
$\|S0\rangle \xrightarrow{I_{Probe}(\tau)} \|T\rangle + ABS, T$	k_{Direct}	---	$1.8 \cdot 10^{13}$
$\|Y\rangle \xrightarrow{I_{Probe}(\tau)} \|S0\rangle + ESE$	k_{ESE}	[a] $4.8 \cdot 10^{13}$	$4.8 \cdot 10^{13}$
$\|X\rangle \xrightarrow{I_{Probe}(\tau)} \|S0\rangle + ESE$			
$\|T\rangle \xrightarrow{I_{Probe}(\tau)} \|S0\rangle + ESE, T$	k_{Direct}	---	$1.8 \cdot 10^{13}$

$\|Y\rangle \longrightarrow \|X\rangle$	k_{YX}	---	[d] $0.9 \cdot 10^{13}$
$\|X\rangle \longrightarrow \|S0\rangle$	k_{UF-nr}	---	[d] $2.4 \cdot 10^{13}$
$\|X\rangle \longrightarrow \|T\rangle$	k_{ISC}	---	[d] $4.0 \cdot 10^{13}$
$\|Y\rangle \xrightarrow{\|Z1\rangle, I_{Probe}(\tau)} \|Y\rangle + ESA,1$	$k_{ESA,1}$	[b] $4.0 \cdot 10^{13}$	$4.0 \cdot 10^{13}$
$\|X\rangle \xrightarrow{\|Z1\rangle, I_{Probe}(\tau)} \|X\rangle + ESA,1$			
$\|T\rangle \xrightarrow{\|Z1\rangle, I_{Probe}(\tau)} \|T\rangle + ESA,1$			
$\|Y\rangle \xrightarrow{\|Z2\rangle, I_{Probe}(\tau)} \|Y\rangle + ESA,2$	$k_{ESA,2}$	[b] $4.3 \cdot 10^{13}$	$4.3 \cdot 10^{13}$
$\|X\rangle \xrightarrow{\|Z2\rangle, I_{Probe}(\tau)} \|X\rangle + ESA,2$			
$\|T\rangle \xrightarrow{\|Z2\rangle, I_{Probe}(\tau)} \|T\rangle + ESA,2$			
$\|Y\rangle \xrightarrow{\|Z3\rangle, I_{Probe}(\tau)} \|Y\rangle + ESA,3$	$k_{ESA,3}$	[b] $4.2 \cdot 10^{13}$	$4.2 \cdot 10^{13}$
$\|X\rangle \xrightarrow{\|Z3\rangle, I_{Probe}(\tau)} \|X\rangle + ESA,3$			
$\|T\rangle \xrightarrow{\|Z3\rangle, I_{Probe}(\tau)} \|T\rangle + ESA,3$			
$\|Y\rangle \xrightarrow{\|Z4\rangle, I_{Probe}(\tau)} \|Y\rangle + ESA,4$	$k_{ESA,4}$	[b] $3.9 \cdot 10^{13}$	$3.9 \cdot 10^{13}$
$\|X\rangle \xrightarrow{\|Z4\rangle, I_{Probe}(\tau)} \|X\rangle + ESA,4$			
$\|T\rangle \xrightarrow{\|Z4\rangle, I_{Probe}(\tau)} \|T\rangle + ESA,4$			
$\|Y\rangle \xrightarrow{\|Z5\rangle, I_{Probe}(\tau)} \|Y\rangle + ESA,5$	$k_{ESA,5}$	[b] $5.4 \cdot 10^{13}$	$5.4 \cdot 10^{13}$
$\|X\rangle \xrightarrow{\|Z5\rangle, I_{Probe}(\tau)} \|X\rangle + ESA,5$			
$\|T\rangle \xrightarrow{\|Z5\rangle, I_{Probe}(\tau)} \|T\rangle + ESA,5$			
$\|T\rangle \longrightarrow \|S0\rangle + rad$	k_{rad}	[c] $11.0 \cdot 10^{4}$	$10.9 \cdot 10^{4}$
$\|T\rangle \longrightarrow \|S0\rangle$	k_{nr}	[c] $3.2 \cdot 10^{6}$	$3.2 \cdot 10^{6}$

[a] From linear absorption

[b] From transient absorption

[c] From time-resolved photoluminescence lifetime and photoluminescence efficiency measurement

[d] Estimated from simulation

[*] Estimated as a 45 fs pump pulse

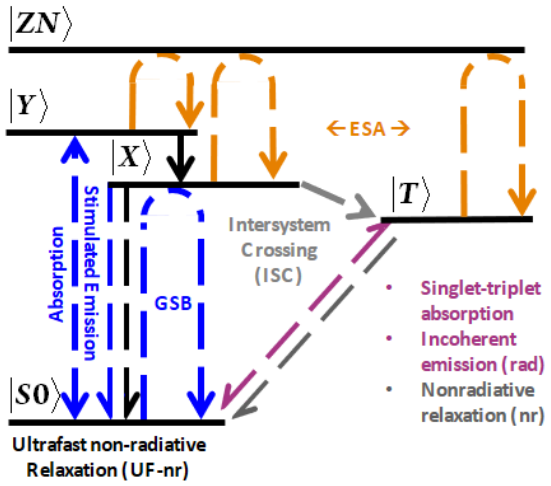

Figure 8. A Jablonski diagram illustrates the optical and non-radiative transitions necessary for simulating the ultrafast photophysics of RuP as described by Model C. Transitions between the electronic ground state and the so-called electronically excited singlet and triplet manifolds are represented in blue and rose respectively. Excited state absorptions are orange and non-radiative pathways are black or gray.

3.5. Using Kinetics Simulations to Estimate Transition Dipoles

The full TA spectrum embodies the multiple optical transitions, as well as non-radiative population channels. Our requirement for quantitative agreement between experimental and simulated full TA spectra provides another layer of validation for it. The full TA spectrum is computed by combining linear and third-order response functions in the slow modulation limit[53-55] with populations from kinetics simulations of the dye photophysics. Transition dipole magnitudes for the absorption from the ground state to the peak excited ^{1}MLCT state $\left|\mu_{Abs}\right|^2$ (D) have been reported,[43] and would be proportional to a global fit of the TA spectrum. By requiring that the predicted and measured TA spectra match, the transition dipole moments associated with the ESAs $\left|\mu_{ESA,m}\right|^2$ can be estimated.

Equations (22)-(25) are the global fit for RuP, representing contributions from the linear absorption, GSB, ESE, and ESAs.

$$S(\omega,\tau)=\sum_j R_j^{(3)}(\omega,\tau)-R^{(1)}(\omega):j\in\{GSB,ESE,ESA\} \tag{21}$$

$$R^{(1)}(\omega)=p_g(-\infty)\cdot\frac{\left|\mu_{Abs}\right|^2}{\hbar\sqrt{2\pi\Delta_{Abs}^2}}\exp\left[-\frac{(\omega-\omega_{Abs})^2}{2\Delta_{Abs}^2}\right] \tag{22}$$

$$R^{(3)}_{GSB}(\omega,\tau)=p_g(\tau)\cdot\frac{|\mu_{Abs}|^4}{2\pi\Delta^2_{Abs}\hbar^3}\exp\left[-\frac{(\omega-\omega_{Abs})^2}{2\Delta^2_{Abs}}\right] \tag{23}$$

$$R^{(3)}_{ESE}(\omega,\tau)=-p_e(\tau)\cdot\frac{|\mu_{Abs}|^4}{2\pi\Delta^2_{Abs}\hbar^3}\exp\left[-\frac{(\omega-\omega_{Abs})^2}{2\Delta^2_{Abs}}\right] \tag{24}$$

$$R^{(3)}_{ESA}(\omega,\tau)=p_{ESA}(\tau)\cdot\sum_m\frac{|\mu_{Abs}|^2|\mu_{ESA,m}|^2}{2\pi\Delta_{Abs}\Delta_{ESA,m}\hbar^3}\exp\left[-\frac{(\omega-\omega_{ESA,m})^2}{2\Delta^2_{ESA,m}}\right]:m\in\{1,2,3,4,5\} \tag{25}$$

The variables p_g, p_e, and p_{ESA} are the associated normalized populations from simulations for the states $|S0\rangle$, $|Y\rangle$, $|X\rangle$, and $|T\rangle$ over the entire range of pump-delay-probe times. For example, when the delay is 0 ps, meaning that the pump and probe pulses are coincident, the calculated populations are as shown in Figure 8. The center frequencies, ω_{Abs} and $\omega_{ESA,m}$, and the variances, Δ^2_{Abs} and $\Delta^2_{ESA,m}$ in wavenumbers (cm^{-1}), are taken directly from the experimental linear absorption and TA spectra.

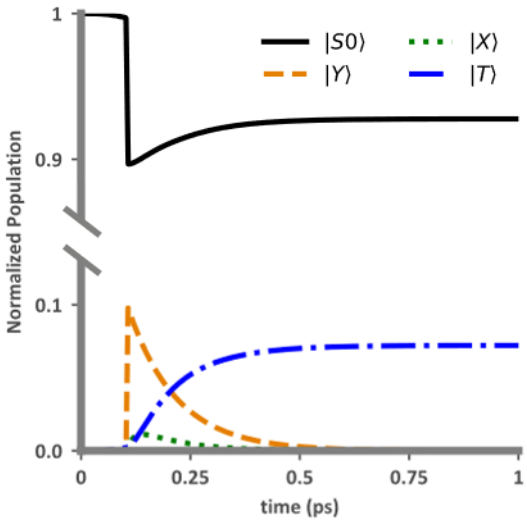

Figure 9. Example of the time-dependent RuP populations for a pump-probe delay time of 0 ps. The ground state (solid black), initially prepared excited singlet state (dashed orange), lowest energy excited singlet state (dotted green), and excited triplet state (dot-dashed blue) populations are normalized to the initial ground state population of 0.4 mM.

4. Results and Discussion

Simulations of the femtosecond TA for chromophore RuP calculated using the scheme in Table 1 describing Model C and initial concentrations and light intensities from experiment are shown in Figure 10 . In panel (A) the GSB, experimental (black) and simulated (blue), reaches a peak intensity of approximately -0.045 followed by ultrafast decay in the signal within 100 fs, and stabilizes to a constant intensity by 300 fs. Similarly, the measured intensities of the ESAs in panels (B)-(F) decay to what appears to be an asymptotic limit within 200-400 fs. Simulated values (orange) demonstrate some decay following time zero, and do achieve agreement at long times. Agreement is satisfactory, especially considering the simplicity of the model as a description of complex vibronic excitations and relaxations in the singlet and triplet manifolds.

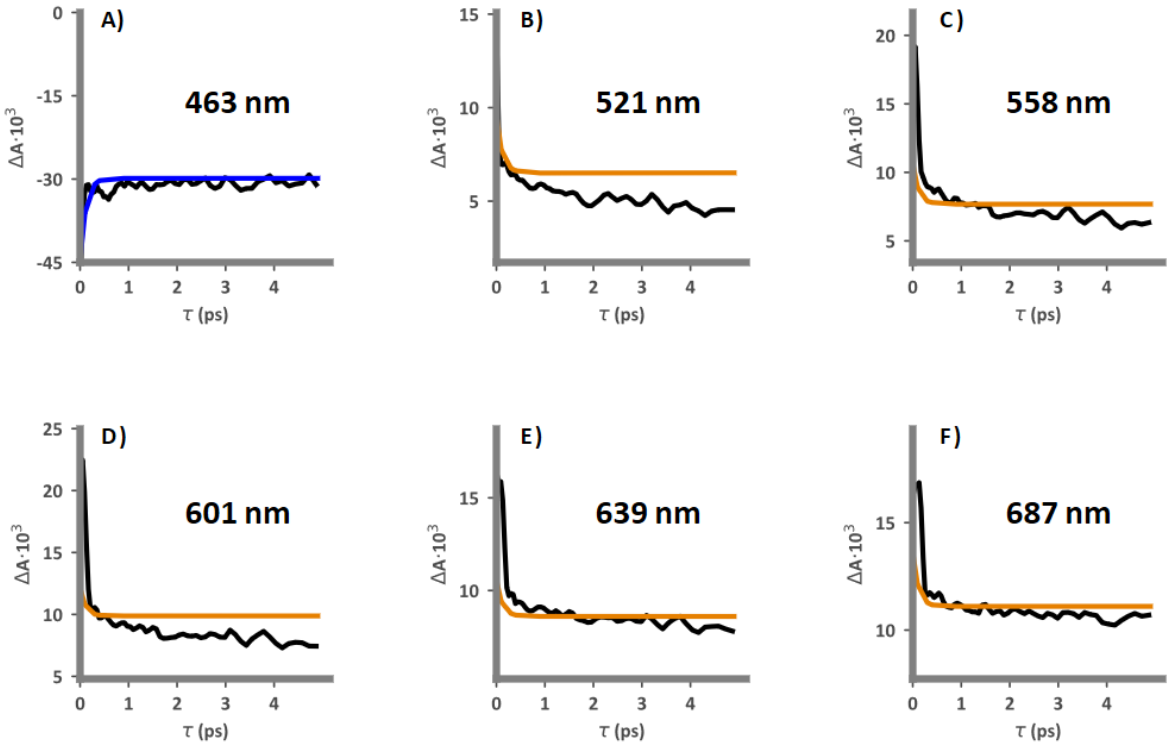

Figure 10. TA time traces of the (A) experimental (black) and simulated (blue) GSB and (B)-(F) experimental (black) and simulated (orange) ESAs for dye RuP.

The success of our kinetic framework is further tested by calculating the full TA signal for RuP, shown in Figure 11. The simulated ground state and excited state populations were used in Equations (21)-(25) to compute the signal in Figure 11B. The experimental and calculated signals at 0 ps and 1 ps are shown in Figure 11C. Estimated transition dipole moment magnitudes are presented in Table 2 for all 6 complexes. Further discussion of the transition dipoles is presented in section 4.3.

Table 2. Estimated transition dipole moment magnitudes for ruthenium complexes.

	RuP	RuP2	RuP3	RuCP	RuCP2	RuCP3
$\|\mu_0\|$ (D)[a]	4.90	6.72	6.90	6.24	6.87	6.48
$\|\mu_1\|$ (D)	5.00	5.93	1.94	6.03	7.13	6.18
$\|\mu_2\|$ (D)	6.61	8.14	4.31	7.58	12.63	8.20
$\|\mu_3\|$ (D)	7.63	9.52	5.74	9.08	16.10	8.80
$\|\mu_4\|$ (D)	6.49	8.62	2.43	5.65	10.11	7.09
$\|\mu_5\|$ (D)	8.10	10.81	5.41	9.40	14.88	8.17

[a] Transition dipole moment magnitudes for ground state to first excited singlet state from reference [43].

At 1-4 ps, both Figures 10B and 10C show that the intensities of the GSB and ESAs at all wavelengths are successfully reproduced. At time zero, the computed GSB is in good agreement with the experiment, while ESA intensities differ at most by 0.005. This is not surprising, given the overall trends in Figure 9B-F. New information on the details of the ESA transitions in the ultrafast regime will be very valuable to understanding the source of this relatively small discrepancy.

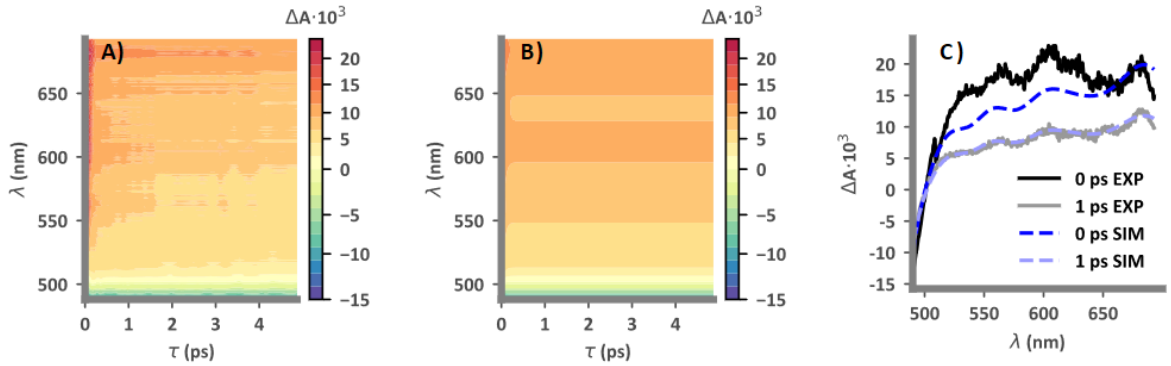

Figure 11. (A) Experimental, (B) simulated, and (C) 0 ps and 1 ps time slices of the TA signal of dye RuP.

4.1. Sensitivity tests for estimated rate coefficients

First-order rate coefficients are a measure of the probability of a unimolecular event occurring per unit of time, however competing transitions involving the same population makes separating out individual rate coefficients from a single apparent first-order coefficient complicated. In this section, we discuss the sensitivity of simulations using our kinetic framework to the values of the rate coefficients estimated in this work. Associated data are presented in full in the Supporting Information section S4.

The laser pulses in a pump-probe experiment are meant to be perturbative, such that the effect on the system is diminishingly small. Purely optical transitions, such as the GSB generated from the ground state population only and the ESAs generated from excited state populations only, can be considered to be fully independent of non-overlapping signal components. Conversely, absorption and emission events move population from one state to another, causing a measurable change in downstream processes. The rate coefficients for processes involved in the GSB (e.g. absorption to state $|X\rangle$, and stimulated emission from the singlet manifolds to the ground state) were varied by an order of magnitude above and below the values shown in Table 3. An increase in the rate coefficients for absorption and stimulated emission decreases the GSB signal somewhat, while a decrease has little effect (Figure S4). The same trend is observed in the ESAs, though to a lesser degree because absorption and emission between singlet states does not directly contribute to the ESA signals. Variations in the rate coefficients of individual ESAs only produce small shifts in the intensity of the associated signal.

The sensitivity of rate coefficients for non-radiative pathways is more pronounced than those of optical transitions. The relaxation of population from state $|Y\rangle$ to state $|X\rangle$ is a bottleneck to both ultrafast non-radiative decay to the ground state and ISC to the excited triplet state. With a 50% decrease in k_{YX}, the peak intensity of the GSB increases by 0.015 and the decay becomes slower, while a 50% increase lowers peak intensity by only 0.005 and the decay is faster (Figure S5(A)). ESAs show a similar influence on peak intensity and lifetime of decay from k_{YX} (Figure S5(B)- (F)).

ISC efficiency ϕ_{ISC} is defined to be the ratio of the rate coefficient for the ISC transition from $|X\rangle$ to $|T\rangle$ to the sum of the rate coefficients for both processes that lead to a decay in $|X\rangle$ population, as shown in Equation (26). ϕ_{ISC} controls TA intensities on the picosecond timescale, when excited states $|Y\rangle$ and $|X\rangle$ have been depopulated. The ESAs show negligible susceptibility to a 3% change in ϕ_{ISC} (Figure S6 (B)-(F)). In contrast, the GSB signal is very sensitive to ϕ_{ISC}. A 3% change

results in a 0.002-0.003 shift in the GSB intensities on the picosecond timescale, as well as changes to peak intensity and the rate of ultrafast decay. It is interesting to note that the simulated TA signals appear to be generally invariant to the values of the individual rate coefficients that make up ϕ_{ISC} so long as the ratio is kept constant (Figure S7).

$$\phi_{ISC} = \frac{k_{ISC}}{k_{uf-nr} + k_{ISC}} \tag{26}$$

For the very slow transitions (incoherent emission and non-radiative relaxation from the excited triplet state), changes in rate coefficients of upstream processes such as optical transitions and relaxation from $|Y\rangle$ to $|X\rangle$ have negligible effects, and the simulated TRPL remained invariant in our sensitivity tests.

4.2. Ligand Effects on the Photophysics

Without alteration, the kinetic steps in the framework developed here (Table 1) were used to simulate TA spectra for the remaining chromophores in Figure 2. This served both as an independent validation test of the mechanism, and as a means to evaluate ligand effects on the ultrafast photophysics of this class of dyes. The detailed simulation results are qualitatively similar to those for RuP, and are presented in full in the Supporting Information, Sections S5.3 and S5.4. We used the same process to estimate rate coefficients for the GSB, absorption, and stimulated emission for the dyes using the linear absorption spectra in Figure S8, and for the ESAs in the TA spectra in Figure S9. Time traces of the dyes are presented in Figure S10 through Figure S14. Figure S15 through Figure S19 present experimental and simulated full TA spectra in panels (A) and (B), and time slices of the TA signal at 0 ps and 1 ps in panel (C).

Simulations of the photophysics of dyes RuP2, RuP3, and RuCP-RuCP3 satisfactorily agree with experimental measurements. While all 5 are similar to chromophore RuP, there are some interesting differences. Unlike RuP, RuCP and RuCP2 do not exhibit ultrafast decay in the GSB; intensity increases slowly over the initial picosecond. GSB intensities for dye RuP2 are much higher than the other chromophores, peaking at -0.075 and decaying to -0.060. ESA1 and ESA2 of RuCP and all ESAs of RuCP2 have an initial slower decay than the other complexes. Similar to RuP, simulation of the TA signal at all wavelengths is in good agreement with experimental values for the remaining dyes, and intensities of the ESAs at times <1 ps are on average lower than those of the measured signals.

Table 3 presents the rate coefficients for all complexes estimated from experiment and used in simulation. Rate coefficients for the ESAs used in the simulations generally fall within 50% of the values estimated from experimental lineshapes, with most less than 20% difference. There are four significant outliers: ESA 4 of dyes RuP3 and RuCP2 and ESA 5 of dyes RuCP and RuCP2 are >80% larger than estimated. Complexes RuP2 and RuCP2 exhibit the most deviation from rate coefficients initially approximated from fits of the TA signal components. The slow non-radiative relaxation and incoherent emission rate coefficients for all dyes differ by less than 1% from those estimated from experiment.

Table 3. Rate coefficients for six ruthenium complexes estimated from experimental data and simulations of time-resolved spectroscopies.

		RuP	RuP2	RuP3	RuCP	RuCP2	RuCP3
GSB	**Experiment (s^{-1})**	$4.8 \cdot 10^{13}$	$3.6 \cdot 10^{13}$	$4.0 \cdot 10^{13}$	$4.1 \cdot 10^{13}$	$4.2 \cdot 10^{13}$	$4.2 \cdot 10^{13}$
	Simulation (s^{-1})	$4.8 \cdot 10^{13}$	$3.6 \cdot 10^{13}$	$4.0 \cdot 10^{13}$	$4.1 \cdot 10^{13}$	$4.2 \cdot 10^{13}$	$4.2 \cdot 10^{13}$
Direct	**Experiment (s^{-1})**	---	---	---	---	---	---
	Simulation (s^{-1})	$1.8 \cdot 10^{13}$	$1.8 \cdot 10^{13}$	$1.8 \cdot 10^{13}$	$1.8 \cdot 10^{13}$	$1.8 \cdot 10^{13}$	$1.8 \cdot 10^{13}$
Y→X	**Experiment (s^{-1})**	---	---	---	---	---	---
	Simulation (s^{-1})	$0.9 \cdot 10^{13}$	$1.2 \cdot 10^{13}$	$4.0 \cdot 10^{13}$	$3.0 \cdot 10^{13}$	$3.0 \cdot 10^{13}$	$3.0 \cdot 10^{13}$
UF-nr	**Experiment (s^{-1})**	---	---	---	---	---	---
	Simulation (s^{-1})	$2.4 \cdot 10^{13}$	$1.0 \cdot 10^{13}$	$4.0 \cdot 10^{13}$	$1.6 \cdot 10^{13}$	$1.6 \cdot 10^{13}$	$2.0 \cdot 10^{13}$
ISC	**Experiment (s^{-1})**	---	---	---	---	---	---
	Simulation (s^{-1})	$4.0 \cdot 10^{13}$	$4.0 \cdot 10^{13}$	$2.0 \cdot 10^{13}$	$2.0 \cdot 10^{13}$	$2.0 \cdot 10^{13}$	$3.6 \cdot 10^{13}$
ESA 1	**Experiment (s^{-1})**	$4.0 \cdot 10^{13}$	$3.8 \cdot 10^{13}$	$4.3 \cdot 10^{13}$	$4.8 \cdot 10^{13}$	$5.2 \cdot 10^{13}$	$4.9 \cdot 10^{13}$
	Simulation (s^{-1})	$4.0 \cdot 10^{13}$	$3.2 \cdot 10^{13}$	$3.8 \cdot 10^{13}$	$4.8 \cdot 10^{13}$	$4.0 \cdot 10^{13}$	$4.9 \cdot 10^{13}$
ESA 2	**Experiment (s^{-1})**	$4.3 \cdot 10^{13}$	$4.0 \cdot 10^{13}$	$4.9 \cdot 10^{13}$	$5.2 \cdot 10^{13}$	$5.7 \cdot 10^{13}$	$5.3 \cdot 10^{13}$
	Simulation (s^{-1})	$4.3 \cdot 10^{13}$	$2.8 \cdot 10^{13}$	$4.7 \cdot 10^{13}$	$5.2 \cdot 10^{13}$	$5.7 \cdot 10^{13}$	$5.3 \cdot 10^{13}$
ESA 3	**Experiment (s^{-1})**	$4.2 \cdot 10^{13}$	$3.9 \cdot 10^{13}$	$5.3 \cdot 10^{13}$	$5.6 \cdot 10^{13}$	$6.2 \cdot 10^{13}$	$5.7 \cdot 10^{13}$
	Simulation (s^{-1})	$4.2 \cdot 10^{13}$	$3.0 \cdot 10^{13}$	$5.3 \cdot 10^{13}$	$5.6 \cdot 10^{13}$	$9.3 \cdot 10^{13}$	$5.7 \cdot 10^{13}$
ESA 4	**Experiment (s^{-1})**	$3.9 \cdot 10^{13}$	$3.7 \cdot 10^{13}$	$2.3 \cdot 10^{13}$	$5.7 \cdot 10^{13}$	$6.1 \cdot 10^{13}$	$5.7 \cdot 10^{13}$
	Simulation (s^{-1})	$3.9 \cdot 10^{13}$	$3.0 \cdot 10^{13}$	$4.6 \cdot 10^{13}$	$5.7 \cdot 10^{13}$	$11 \cdot 10^{13}$	$5.7 \cdot 10^{13}$
ESA 5	**Experiment (s^{-1})**	$5.4 \cdot 10^{13}$	$5.1 \cdot 10^{13}$	$4.8 \cdot 10^{13}$	$3.6 \cdot 10^{13}$	$4.5 \cdot 10^{13}$	$3.4 \cdot 10^{13}$
	Simulation (s^{-1})	$5.4 \cdot 10^{13}$	$3.8 \cdot 10^{13}$	$5.0 \cdot 10^{13}$	$7.0 \cdot 10^{13}$	$10.5 \cdot 10^{13}$	$5.0 \cdot 10^{13}$
	Experiment (s^{-1})	$11 \cdot 10^{4}$	$9.6 \cdot 10^{4}$	$11 \cdot 10^{4}$	$10.6 \cdot 10^{4}$	$10.2 \cdot 10^{4}$	$10.3 \cdot 10^{4}$

Incoherent Emission	**Simulation (s^{-1})**	$10.9 \cdot 10^4$	$9.6 \cdot 10^4$	$11 \cdot 10^4$	$10.6 \cdot 10^4$	$10.6 \cdot 10^4$	$10.3 \cdot 10^4$
Non-radiative Relaxations	**Experiment (s^{-1})**	$3.2 \cdot 10^6$	$2.6 \cdot 10^6$	$2.0 \cdot 10^6$	$2.0 \cdot 10^6$	$2.1 \cdot 10^6$	$2.4 \cdot 10^6$
	Simulation (s^{-1})	$3.2 \cdot 10^6$	$2.6 \cdot 10^6$	$2.0 \cdot 10^6$	$2.0 \cdot 10^6$	$2.2 \cdot 10^6$	$2.3 \cdot 10^6$

Rate coefficients for radiative and non-radiative transitions, with the obvious exception of those for the incoherent emission and slow repopulation of the ground state, are all approximately within an order of magnitude of each other, 10^{13} s^{-1}. The relative importance of competing pathways depends on rates: if their rate coefficients are similar, instantaneous populations are the more important factor in determining rates and branching ratios. This is illustrated in Figure 12, which shows time dependent concentrations at simulated pump-probe delays of 0 ps (solid black), 0.5 ps (dashed orange), 1 ps (dotted green), and 5 ps (dash-dotted blue) of the (A) ground state, (B) initially prepared excited singlet state, (C) lowest energy excited singlet state, and (D) excited triplet state. This example also illustrates the complexity of probe-induced excitations that open parallel kinetic pathways that affect the dye populations. The concentration of dyes in the initially prepared excited singlet state $|\boldsymbol{Y}\rangle$ is seemingly invariant to length of the delay, Figure 12B. This is because the probe does not promote ground state population to $|\boldsymbol{Y}\rangle$, it only induces a stimulated emission. Upon the arrival of the probe pulse, ~1% of the ground state population is excited to the state $|\boldsymbol{X}\rangle$, and ~0.5% is promoted to $|\boldsymbol{T}\rangle$. Such proportions are a small perturbation for $|\boldsymbol{S0}\rangle$, but as seen in Figure 12 panels (C) and (D) they result in a relative change in population for $|\boldsymbol{X}\rangle$ of ~10% and a cumulative increase in population to $|\boldsymbol{T}\rangle$ of ~15%. Since excited state populations govern the extent of stimulated emission and the ESAs, such significant changes in concentration should not be neglected.

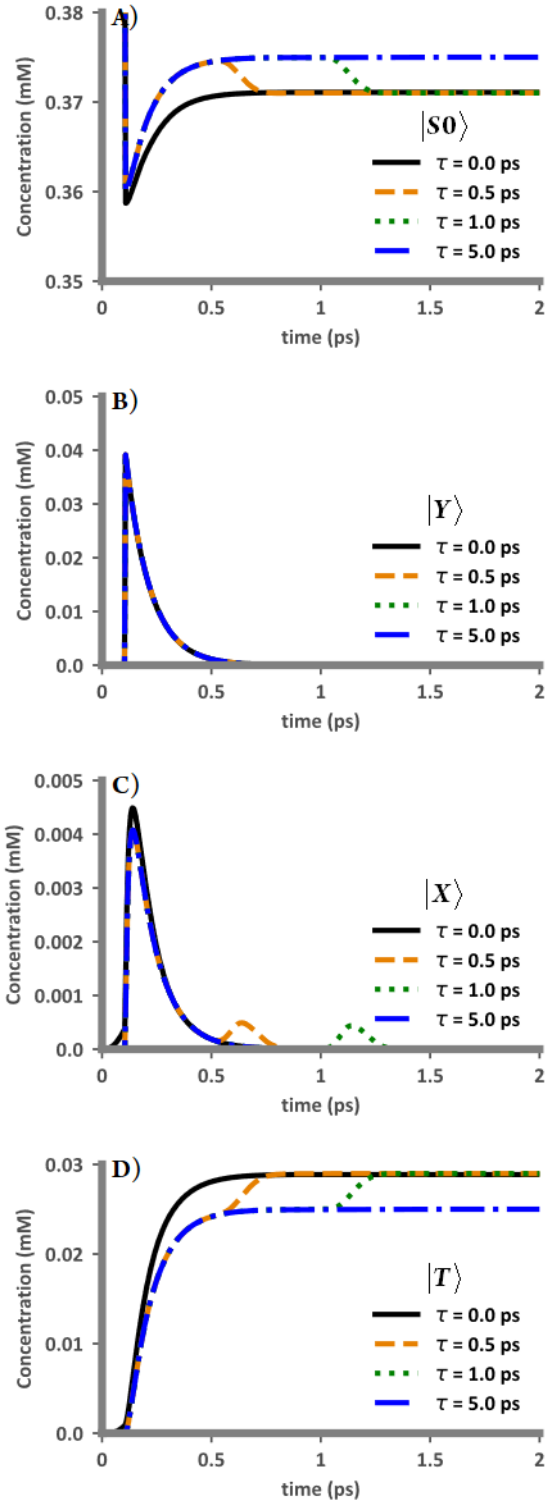

Figure 12. Time dependent concentration with a pump-probe delay of 0 ps (solid black), 0.5 ps (dashed orange), 1 ps (dotted green), and 5 ps (dash-dotted blue) for (A) ground state, (B) initially prepared excited singlet state, (C) lowest energy excited singlet state, and (D) excited triplet state.

Table 4 shows the computed ϕ_{ISC} for all six dyes. These ISC efficiencies yield the best agreement between experimental and simulated GSB signal components. The rate coefficients for the ESA optical transitions used

Table 4. Estimated intersystem crossing efficiencies for six ruthenium complexes.

Dye	ϕ_{ISC}
RuP	0.63
RuP2	0.80
RuP3	0.33
RuCP	0.56
RuCP2	0.56
RuCP3	0.64

in the simulations are upper limits for all dyes except RuP2, suggesting that ϕ_{ISC} values could be greater for RuP, RuP3 and RuCP-RuCP3, and smaller for RuP2. For dyes RuCP-RuCP3 the calculated efficiencies are similar, providing evidence that addition of the methyl spacers between the bipyridine ligands and the phosphonates may serve to isolate excitations to the central RuBPY structure, and thus minimize phosphonate effects on relaxations. It is significant to note that the efficiency for ISC in RuBPY is generally accepted to be unity,[20, 23-24, 56] yet we are estimating efficiencies for a set of RuBPY derivatives to be 20-50% smaller. Moreover, the ultrafast decays of the GSB and ESAs are intimately connected with ϕ_{ISC} . One possible explanation for the apparent discrepancy between conclusions drawn from our simulation and previous experimental studies is that the kinetic framework does not include sub-picosecond fluorescence as an explicit mechanistic step, although it has been reported previously.[29, 37] The impact of fluorescence on populations could be accounted for implicitly in the rate coefficients for optical transitions of ESAs within 500-550 nm, however. If this were in fact the case, what is often referred to as the efficiency of ISC would be the efficiency of IC to an emitting state as was originally proposed.[19, 22]

4.3. Transition Dipoles

Transition dipoles for excited state optical transitions $|\mu_1|$-$|\mu_s|$, associated with the five ESAs, were estimated by using the simulated populations and transition dipole magnitudes for singlet-singlet transitions $|\mu_0|$ as described in the beginning

of Section 4. The transition dipole magnitudes between ground state and excited singlet state used to estimate $|\mu_1|$-$|\mu_s|$ in Table 2 were computed from resonant Raman analysis of the dyes,[43] and within error are equivalent to values reported from Stark spectroscopy for closely related Ru dyes.[57-58] RuP2 and RuCP2 have the largest excited state transition dipole magnitudes. The values estimated for RuP and RuCP are comparable, but anomalously low magnitudes for dye RuP3 hinder evaluation against RuCP3 and across the P series and CP series.

The transition dipole moment magnitudes (Table 2) and efficiencies for ISC (Table 4) for the P and CP series suggest that while the kinetics observed for these chromophores are generally comparable, at first glance the estimated values do not follow a simple trend. However, as shown in panels (A)-(E) of Figure 13, for ESA 1-5, the magnitudes of the transition dipole moments appear to be positively correlated with ϕ_{ISC} of each dye. This trend is outside of our estimated standard deviations from the sensitivity studies, which are within 0.1-0.3 D for ESAs 1-3 and 5, and between 1 and 3 D for ESA 4. Physically, this indicates that the probability of ISC relative to ultrafast relaxation and the probability of ESA are related. It is possible that ϕ_{ISC} is likely most facilitated by a large SOC, which increases the mixing of spin character, rendering multiplicity a poor quantum number for such cases. If this is the case, relaxation of the selection rule applying to states with singlet and triplet character could increase ESA.

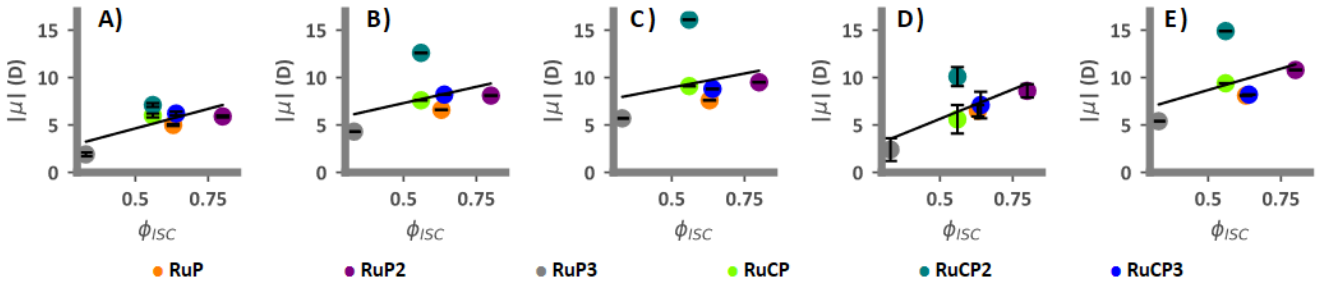

Figure 13. Transition dipole magnitudes plotted against ISC efficiency for (A) ESA 1, (B) ESA 2, (C) ESA 3, (D) ESA 4, and (E) ESA 5. Error is smaller than marker size for all ESA except ESA 4.

The efficiency of PL was closely correlated to the efficiency of ISC in early studies of RuBPY, in part because the emitting state was purported to have pure spin.[20, 24, 27] Later work suggesting mixed multiplicity in the states of RuBPY,[33-34] which calls into question what is meant by ISC for such a molecule. Ultrafast decay in the GSB was observed for four of the

six dyes that experimental data are available for, and femtosecond to picosecond decay in the ESAs for all dyes. This suggests that there is a decay channel of the GSB that does not traverse the so-called triplet manifold, and therefore ϕ_{ISC} cannot be unity. By including an ultrafast transition to the ground state in our kinetic framework, good agreement with the intensities of the GSB and ESAs is realized on the picosecond timescale. The probability often referred to by ϕ_{ISC} would be more appropriately defined as the efficiency of excited state relaxation to an emitting state. Although the ultrafast decay mechanism adopted in this kinetic framework is non-radiative, there is literature precedence for luminescence from states primarily singlet in character.[29, 59]

The kinetic analysis of time-resolved spectroscopies have yielded new insights into RuBPY and its derivatives, but there is still much to be learned. Beyond TA, multidimensional spectroscopies and the accompanying analyses can provide a breadth of knowledge. Two dimensional electronic-vibrational spectroscopy[60] and pump-push-probe spectroscopy[61] can be used to understand the transition, and thus the nature of the states, between $|Y\rangle$ and $|X\rangle$. Pump-repump-probe[62-63] measurements could add further clarity to the photophysical picture, while theory could shed light on the nature of non-adiabatic transitions on the femtosecond timescale. Inventive studies connecting multiple datasets[43, 64-65] and meta-analyses across many investigations[10] can yield new insights and bring together perspectives from across disciplines.

5. Conclusion

We have developed a kinetic framework that simulates the optical transitions and non-radiative relaxation pathways of the dyes in Figure 2 that are in good agreement with experimental time traces, reproducing ultrafast dynamics and downstream processes. The simulations reveal that an ultrafast relaxation pathway competes with intersystem crossing to the triplet state, resulting in an ISC efficiency less than unity. Rate coefficients estimated directly from experiment and estimated from experimental constraints are on the order of 10^{13} s^{-1}. Validation of our kinetic framework by successfully simulating multiple cases across this class of chromophores suggests that the proposed model is predictive. Using simulated populations as a function of time, a global analysis of the optical data provides new estimates of the transition dipole moment magnitudes for excited state transitions. These results are not accessible with the more commonly used techniques for analysis of time resolved spectroscopies, in which phenomenological lifetimes are extracted from experimental time-resolved data using a sum-of-exponentials analysis that assumes first-order dynamic events that are well separated in time.

The ruthenium chromophores examined here exhibit photoinduced relaxation dynamics involving coincident transitions and multiple populations contributing to the same observables, making such simplifying assumptions unjustifiable. The kinetic model, which fully connects measurements to primary photophysical processes, shows the importance of integrating the characteristics of the measurement, even within the perturbative regime, into any analytical approach designed to extract fundamental insights. The generalizability of this kinetic framework makes it ideally applicable to a broad class of photophysical and photochemical systems. In particular, it can be extended to include charge injection into a substrate, interactions with the catalyst, or electrolyte-driven quenching.

ASSOCIATED CONTENT

Supporting Information. Presented: lineshape of simulated probe profiles; figures comparing ground state bleach and excited state absorptions of several models; figures showing sensitivity tests of the ground state bleach and excited state absorptions; linear absorption for six dyes; transient absorption at 1 ps for six dyes; experimental and simulated time traces of the ground state bleach and excited state absorptions for six dyes; and experimental and simulated full transient absorption signals and time slices at 0 ps and 1 ps. Additionally, an Excel spreadsheet with main document figure data is available. This material is available free of charge via the Internet at http://pubs.acs.org.

AUTHOR INFORMATION

Corresponding Author

*Author to whom correspondence should be addressed, fahoule@lbl.,gov

Notes

FAH and TJM conceived of this study. AMM, JMP, GJM and TJM provided data and experimental details and participated in interpretation of the simulation results. AMM was the graduate advisor of PGG. JMP was the postdoctoral advisor of DFZ. TPC wrote the first draft of the manuscript. All authors have given approval to the final version of the manuscript.

ACKNOWLEDGMENT

This material is based upon work supported by the U.S. Department of Energy, Office of Science, Office of Basic Energy Sciences, Chemical Sciences, Geosciences, and Biosciences Division, in the Solar Photochemistry Program under Contract No. DE-AC02-05CH11231 (supporting TPC and FAH, who developed the kinetic framework for the ultrafast photophysics of RuBPY derivatives in solution). MKB (compiled TA and TRPL data for analysis and interpreted simulated TA GSB signals of RuBPY derivatives) and DFZ (interpreted simulated TA GSB signals of RuBPY derivatives) and a study by PGG (performed fs-TA measurements and provided essential experimental details) were supported by the Alliance for Molecular PhotoElectrode Design for Solar Fuels (AMPED), an Energy Frontier Research Center (EFRC) funded by the U.S. Department of Energy, Office of Science, Office of Basic Energy Sciences under Award Number DE-SC0001011.

REFERENCES

1. Gerischer, H.; Tributsch, H., Elektrochemische Untersuchungen Zur Spektralen Sensibilisierung Von Zno-Einkristallen. *Berichte der Bunsengesellschaft für physikalische Chemie* **1968,** *72*, 437-445.

2. Gerischer, H.; Michel-Beyerle, M. E.; Rebentrost, F.; Tributsch, H., Sensitization of Charge Injection into Semiconductors with Large Band Gap. *Electrochim. Acta* **1968,** *13*, 1509-1515.

3. Matsumura, M.; Matsudaira, S.; Tsubomura, H.; Takata, M.; Yanagida, H., Dye Sensitization and Surface-Structures of Semiconductor Electrodes. *Ind. Eng. Chem. Prod. Res. Dev.* **1980,** *19*, 415-421.

4. Tributsch, H., Reaction of Excited Chlorophyll Molecules at Electrodes and in Photosynthesis. *Photochem. Photobiol.* **1972,** *16*, 261-269.

5. Tributsch, H.; Calvin, M., Electrochemistry of Excited Molecules - Photo-Electrochemical Reactions of Chlorophylls. *Photochem. Photobiol.* **1971,** *14*, 95-112.

6. Brown, A. M.; McCusker, C. E.; Carey, M. C.; Blanco-Rodriguez, A. M.; Towrie, M.; Clark, I. P.; Vlcek, A.; McCusker, J. K., Vibrational Relaxation and Redistribution Dynamics in Ruthenium(Ii) Polypyridyl-Based Charge-Transfer Excited States: A Combined Ultrafast Electronic and Infrared Absorption Study. *J. Phys. Chem. A* **2018,** *122*, 7941-7953.

7. Eberhart, M. S.; Bowers, L. M. R.; Shan, B.; Troian-Gautier, L.; Brennaman, M. K.; Papanikolas, J. M.; Meyer, T. J., Completing a Charge Transport Chain for Artificial Photosynthesis. *J. Am. Chem. Soc.* **2018,** *140*, 9823-9826.

8. Xu, P.; Gray, C. L.; Xiao, L.; Mallouk, T. E., Charge Recombination with Fractional Reaction Orders in Water-Splitting Dye-Sensitized Photoelectrochemical Cells. *J. Am. Chem. Soc.* **2018,** *140*, 11647-11654.

9. Xu, P. T.; Mallouk, T. E., Charge Transfer Dynamics in Aqueous Dye-Sensitized Photoelectrochemical Cells: Implications for Water Splitting Efficiency. *J. Phys. Chem. C* **2019,** *123*, 299-305.

10. Zigler, D. F.; Morseth, Z. A.; Wang, L.; Ashford, D. L.; Brennaman, M. K.; Grumstrup, E. M.; Brigham, E. C.; Gish, M. K.; Dillon, R. J.; Alibabaei, L., et al., Disentangling the Physical Processes Responsible for the Kinetic Complexity in Interfacial Electron Transfer of Excited Ru(Ii) Polypyridyl Dyes on Tio2. *J. Am. Chem. Soc.* **2016,** *138*, 4426-38.

11. Campbell, W. M.; Burrell, A. K.; Officer, D. L.; Jolley, K. W., Porphyrins as Light Harvesters in the Dye-Sensitised Tio2 Solar Cell. *Coord. Chem. Rev.* **2004,** *248*, 1363-1379.

12. Carella, A.; Borbone, F.; Centore, R., Research Progress on Photosensitizers for Dssc. *Front. Chem.* **2018,** *6*, 481.

13. Hagberg, D. P.; Marinado, T.; Karlsson, K. M.; Nonomura, K.; Qin, P.; Boschloo, G.; Brinck, T.; Hagfeldt, A.; Sun, L., Tuning the Homo and Lumo Energy Levels of Organic Chromophores for Dye Sensitized Solar Cells. *J. Org. Chem.* **2007,** *72*, 9550-6.

14. McCusker, J. K., Electronic Structure in the Transition Metal Block and Its Implications for Light Harvesting. *Science* **2019,** *363*, 484-488.

15. Crosby, G. A.; Perkins, W. G.; Klassen, D. M., Luminescence from Transition-Metal Complexes: Tris(2,2'-Bipyridine)- and Tris(1,10-Phenanthroline)Ruthenium(Ii). *J. Chem. Phys.* **1965,** *43*, 1498-1503.

16. Demas, J. N.; Crosby, G. A., On the Multiplicity of the Emitting State of Ruthenium(Ii) Complexes. *J. Mol. Spectrosc.* **1968,** *26*, 72-77.

17. Klassen, D. M.; Crosby, G. A., Reassignment of the Luminescence from Ruthenium(Iii) Complexes. *Chem. Phys. Lett.* **1967,** *1*, 127-128.

18. Klassen, D. M.; Crosby, G. A., Spectroscopic Studies of Ruthenium(Ii) Complexes. Assignment of the Luminescence. *J. Chem. Phys.* **1968,** *48*, 1853-1858.

19. Paris, J. P.; Brandt, W. W., Charge Transfer Luminescence of a Ruthenium(Ii) Chelate. *J. Am. Chem. Soc.* **1959,** *81*, 5001-5002.

20. Lytle, F. E.; Hercules, D. M., Luminescence of Tris(2,2'-Bipyridine)Ruthenium(Ii) Dichloride. *J. Am. Chem. Soc.* **1969,** *91*, 253-257.

21. Crosby, G. A., Spectroscopic Investigations of Excited-States of Transition-Metal Complexes. *Acc. Chem. Res.* **1975,** *8*, 231-238.

22. Crosby, G. A.; Demas, J. N., Quantum Efficiencies on Transition Metal Complexes. Ii. Charge-Transfer Luminescence. *J. Am. Chem. Soc.* **1971,** *93*, 2841-2847.

23. Laurence, G. S.; Balzani, V., Reduction by the Triplet Charge-Transfer State of Tris(Bipyridyl)Ruthenium(Ii). Photochemical Reaction between Tris(Bipyridyl) Ruthenium(Ii) and Thallium(Iii). *Inorg. Chem.* **2002,** *13*, 2976-2982.

24. Wrighton, M.; Markham, J., Quenching of the Luminescent State of Tris(2,2'-Bipyridine)Ruthenium(Ii) by Electronic Energy Transfer. *J. Phys. Chem.* **1973,** *77*, 3042-3044.

25. Bensasson, R.; Salet, C.; Balzani, V., Laser Flash Spectroscopy of Tris(2,2'-Bipyridine)Ruthenium(Ii) in Solution. *J. Am. Chem. Soc.* **1976,** *98*, 3722-3724.

26. Bolletta, F.; Maestri, M.; Balzani, V., Efficiency of the Intersystem Crossing from the Lowest Spin-Allowed to the Lowest Spin-Forbidden Excited State of Some Chromium(Iii) and Ruthenium(Ii) Complexes. *J. Phys. Chem.* **1976,** *80*, 2499-2503.

27. Demas, J. N.; Taylor, D. G., On the "Intersystem Crossing" Yields in Ruthenium(Ii) and Osmium(Ii) Photosensitizers. *Inorg. Chem.* **2002,** *18*, 3177-3179.

28. Michael-Grätzel, M. M., 530 Nm-Laser Photolysis Studies of the Photo Reduction of Tris (2,2-Bipyridine)-Ruthenium(Ii) by Organic Donors. *Berichte der Bunsengesellschaft für physikalische Chemie* **1977,** *81*, 504-507.

29. Cannizzo, A.; van Mourik, F.; Gawelda, W.; Zgrablic, G.; Bressler, C.; Chergui, M., Broadband Femtosecond Fluorescence Spectroscopy of [Ru(Bpy)3]2+. *Angew. Chem. Int. Ed. Engl.* **2006,** *45*, 3174-6.

30. Damrauer, N. H.; Cerullo, G.; Yeh, A.; Boussie, T. R.; Shank, C. V.; McCusker, J. K., Femtosecond Dynamics of Excited-State Evolution In. *Science* **1997,** *275*, 54-7.

31. Felix, F.; Ferguson, J.; Guedel, H. U.; Ludi, A., The Electronic Spectrum of Tris(2,2'-Bipyridine)Ruthenium(2+). *J. Am. Chem. Soc.* **1980,** *102*, 4096-4102.

32. Malouf, G.; Ford, P. C., Photochemistry of the Ruthenium(Ii) Ammine Complexes, Ru(Nh3)5(Py-X)2+. Variation of Systemic Parameters to Modify Photochemical Reactivities. *J. Am. Chem. Soc.* **1977,** *99*, 7213-7221.

33. Kober, E. M.; Meyer, T. J., Concerning the Absorption Spectra of the Ions M(Bpy)32+ (M = Fe, Ru, Os; Bpy = 2,2'-Bipyridine). *Inorg. Chem.* **1982,** *21*, 3967-3977.

34. Daul, C.; Baerends, E. J.; Vernooijs, P., A Density-Functional Study of the Mlct States of [Ru(Bpy)3]2+ in D3 Symmetry. *Inorg. Chem.* **1994,** *33*, 3538-3543.

35. Damrauer, N. H.; McCusker, J. K., Ultrafast Dynamics in the Metal-to-Ligand Charge Transfer Excited-State Evolution of [Ru(4,4'-Diphenyl-2,2'-Bipyridine)3]2+. *J. Phys. Chem. A* **1999,** *103*, 8440-8446.

36. Dongare, P.; Myron, B. D. B.; Wang, L.; Thompson, D. W.; Meyer, T. J., [Ru(Bpy)3]2+* Revisited. Is It Localized or Delocalized? How Does It Decay? *Coord. Chem. Rev.* **2017,** *345*, 86-107.

37. Henry, W.; Coates, C. G.; Brady, C.; Ronayne, K. L.; Matousek, P.; Towrie, M.; Botchway, S. W.; Parker, A. W.; Vos, J. G.; Browne, W. R., et al., The Early Picosecond Photophysics of Ru(Ii) Polypyridyl Complexes: A Tale of Two Timescales. *J. Phys. Chem. A* **2008,** *112*, 4537-44.

38. Hewitt, J. T.; Vallett, P. J.; Damrauer, N. H., Dynamics of the 3mlct in Ru(Ii) Terpyridyl Complexes Probed by Ultrafast Spectroscopy: Evidence of Excited-State Equilibration and Interligand Electron Transfer. *J. Phys. Chem. A* **2012,** *116*, 11536-47.

39. Shaw, G. B.; Brown, C. L.; Papanikolas, J. M., Investigation of Interligand Electron Transfer in Polypyridyl Complexes of Os(Ii) Using Femtosecond Polarization Anisotropy Methods: Examination of Os(Bpy)32+and Os(Bpy)2(Mab)2+. *J. Phys. Chem. A* **2002,** *106*, 1483-1495.

40. Shaw, G. B.; Styers-Barnett, D. J.; Gannon, E. Z.; Granger, J. C.; Papanikolas, J. M., Interligand Electron Transfer Dynamics in [Os(Bpy)(3)](2+): Exploring the Excited State Potential Surfaces with Femtosecond Spectroscopy. *J. Phys. Chem. A* **2004,** *108*, 4998-5006.

41. Wallin, S.; Davidsson, J.; Modin, J.; Hammarstrom, L., Femtosecond Transient Absorption Anisotropy Study on [Ru(Bpy)3]2+ and [Ru(Bpy)(Py)4]2+. Ultrafast Interligand Randomization of the Mlct State. *J. Phys. Chem. A* **2005,** *109*, 4697-704.

42. Bunker, D. L., Simple Kinetic Models from Arrhenius to the Computer. *Acc. Chem. Res.* **2002,** *7*, 195-201.

43. Giokas, P. G.; Miller, S. A.; Hanson, K.; Norris, M. R.; Glasson, C. R. K.; Concepcion, J. J.; Bettis, S. E.; Meyer, T. J.; Moran, A. M., Spectroscopy and Dynamics of Phosphonate-Derivatized Ruthenium Complexes on Tio2. *J. Phys. Chem. C* **2013,** *117*, 812-824.

44. Hanson, K.; Brennaman, M. K.; Ito, A.; Luo, H.; Song, W.; Parker, K. A.; Ghosh, R.; Norris, M. R.; Glasson, C. R. K.; Concepcion, J. J., et al., Structure–Property Relationships in Phosphonate-Derivatized, Ruii Polypyridyl Dyes on Metal Oxide Surfaces in an Aqueous Environment. *J. Phys. Chem. C* **2012,** *116*, 14837-14847.

45. Foggi, P.; Bussotti, L.; Neuwahl, F. V. R., Photophysical and Photochemical Applications of Femtosecond Time-Resolved Transient Absorption Spectroscopy. *Int. J. Photoenergy* **2001,** *3*.

46. Hinsberg, W. D.; Houle, F. A. Kinetiscope. http://hinsberg.net/kinetiscope/ (accessed Apr. 2020).

47. Bunker, D. L.; Garrett, B.; Kleindienst, T.; Long, G. S., Discrete Simulation Methods in Combustion Kinetics. *Combust. Flame* **1974,** *23*, 373-379.

48. Gillespie, D. T., A General Method for Numerically Simulating the Stochastic Time Evolution of Coupled Chemical Reactions. *J. Comput. Phys.* **1976,** *22*, 403-434.

49. Yoon, S.; Kukura, P.; Stuart, C. M.; Mathies, R. A., Direct Observation of the Ultrafast Intersystem Crossing in Tris(2,2′-Bipyridine)Ruthenium(Ii) Using Femtosecond Stimulated Raman Spectroscopy. *Mol. Phys.* **2006,** *104*, 1275-1282.

50. Yamaguchi, S.; Hamaguchi, H. O., Convenient Method of Measuring the Chirp Structure of Femtosecond White-Light Continuum Pulses. *Appl. Spectrosc.* **1995,** *49*, 1513-1515.

51. Thompson, D. W.; Ito, A.; Meyer, T. J., [Ru(Bpy)3]2+* and Other Remarkable Metal-to-Ligand Charge Transfer (Mlct) Excited States. *Pure Appl. Chem.* **2013,** *85*, 1257-1305.

52. Hilborn, R. C., Einstein Coefficients, Cross-Sections, F Values, Dipole-Moments, and All That. *Am. J. Phys.* **1982,** *50*, 982-986.

53. Kelley, A. M., *Condensed-Phase Molecular Spectroscopy and Photophysics*. Wiley Online Library: 2013.

54. Mukamel, S., *Principles of Nonlinear Optical Spectroscopy*. Oxford University Press on Demand: 1999.

55. Valkunas, L.; Abramavicius, D.; Mancal, T., *Molecular Excitation Dynamics and Relaxation: Quantum Theory and Spectroscopy*. John Wiley & Sons: 2013.

56. Demas, J. N.; Crosby, G. A., Measurement of Photoluminescence Quantum Yields - Review. *J. Phys. Chem.* **1971,** *75*, 991-1024.

57. Maurer, A. B.; Piechota, E. J.; Meyer, G. J., Excited-State Dipole Moments of Homoleptic [Ru(Bpy')3](2+) Complexes Measured by Stark Spectroscopy. *J. Phys. Chem. A* **2019,** *123*, 8745-8754.

58. Oh, D. H.; Boxer, S. G., Stark-Effect Spectra of Ru(Diimine)32+ Complexes. *J. Am. Chem. Soc.* **1989,** *111*, 1130-1131.

59. Harriman, A.; Izzet, G., Direct Observation of the Fourth Mlct Triplet State in Ruthenium(Ii) Tris(2,2'-Bipyridine). *Phys. Chem. Chem. Phys.* **2007,** *9*, 944-8.

60. Oliver, T. A.; Lewis, N. H.; Fleming, G. R., Correlating the Motion of Electrons and Nuclei with Two-Dimensional Electronic-Vibrational Spectroscopy. *Proc Natl Acad Sci U S A* **2014,** *111*, 10061-6.

61. Paternò, G. M.; Moretti, L.; Barker, A. J.; Chen, Q.; Müllen, K.; Narita, A.; Cerullo, G.; Scotognella, F.; Lanzani, G., Pump–Push–Probe for Ultrafast All-Optical Switching: The Case of a Nanographene Molecule. *Adv. Funct. Mater.* **2018,** *29*, 1805249.

62. Nuernberger, P.; Ruetzel, S.; Brixner, T., Multidimensional Electronic Spectroscopy of Photochemical Reactions. *Angew. Chem. Int. Ed. Engl.* **2015,** *54*, 11368-86.

63. Snyder, J. A.; Bragg, A. E., Ultrafast Pump-Repump-Probe Photochemical Hole Burning as a Probe of Excited-State Reaction Pathway Branching. *J Phys Chem Lett* **2018,** *9*, 5847-5854.

64. Kelley, A. M., Resonance Raman Intensity Analysis of Vibrational and Solvent Reorganization in Photoinduced Charge Transfer. *J. Phys. Chem. A* **1999,** *103*, 6891-6903.

65. Moran, A. M.; Kelley, A. M., Solvent Effects on Ground and Excited Electronic State Structures of P-Nitroaniline. *J. Chem. Phys.* **2001,** *115*, 912-924.

TOC Graphic

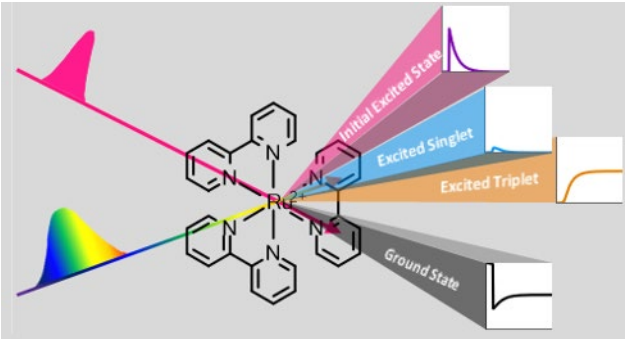
Initial Excited State
Excited Singlet
Excited Triplet
Ground State
N
N
N
N
N
N
Ru2+